Latin American Journal of Solids and Structures
www.lajss.org

Strain Rate Dependent Behavior and Modeling for Compression Response of Hybrid Fiber Reinforced Concrete

Abstract

This paper investigates the stress-strain characteristics of Hybrid fiber reinforced concrete (HFRC) composites under dynamic compression using Split Hopkinson Pressure Bar (SHPB) for strain rates in the range of 25 to 125 s^{-1}. Three types of fibers – hooked ended steel fibers, monofilament crimped polypropylene fibers and staple Kevlar fibers were used in the production of HFRC composites. The influence of different fibers in HFRC composites on the failure mode, dynamic increase factor (DIF) of strength, toughness and strain are also studied. Degree of fragmentation of HFRC composite specimens increases with increase in the strain rate. Although the use of high percentage of steel fibers leads to the best performance but among the hybrid fiber combinations studied, HFRC composites with relatively higher percentage of steel fibers and smaller percentage of polypropylene and Kevlar fibers seem to reflect the equally good synergistic effects of fibers under dynamic compression. A rate dependent analytical model is proposed for predicting complete stress-strain curves of HFRC composites. The model is based on a comprehensive fiber reinforcing index and complements well with the experimental results.

Keywords

Hybrid fibers; Concrete; FRC; SHPB; Strain rate; Toughness; Reinforcing index; Stress-strain curve; DIF.

S.M. Ibrahim [a]
Tarek H. Almusallam [a]
Yousef A. Al-Salloum [a]
Aref A. Abadel [a]
Husain Abbas [a*]

[a] MMB Chair of Research and Studies in Strengthening and Rehabilitation of Structures, Department of Civil Engineering, King Saud University, Riyadh 11421, Saudi Arabia.

*Author email:
abbas_husain@hotmail.com.

http://dx.doi.org/10.1590/1679-78252717

Received 17.12.2015
In revised form 09.03.2016
Accepted 04.04.2016
Available online 12.04.2016

1 INTRODUCTION

Hybrid fiber reinforced concrete (HFRC) composite is a mix of concrete matrix and fibers with different material and geometric properties that results in synergistic and superior performance compared to the use of only one type of fibers in concrete composites. Strong and stiff fibers (e.g. steel fibers, Kevlar fibers) can restrain micro-crack growth, thus improving the concrete strength, whereas relatively flexible fibers (e.g. Polypropylene fibers, Polyethylene fibers, Polyvinyl alcohol) improve material toughness by stress transfer mechanisms over larger crack openings (Abadel et al.,

2015; Almusallam et al., 2013; Almusallam et al., 2014; Bolander et al., 2008). Some of the obvious advantages of the HFRC composites in construction practices are improved homogeneity, better crack management, possibility of slender structural members (Almusallam et al., 2013, 2014; Yu et al., 2014; Markovic et al., 2006). However, to ensure a balance between ultimate strength and strain capacity, optimum volume/weight proportion of different fibers is desired (Ahmed et al., 2007). For static loading conditions, HFRC composites result in better energy absorbing properties compared with that of mono-fiber concrete composites (Chen et al., 1996; Abou El-Mal et al., 2015; Li, 2012). A new type of steel fiber with spiral shape, proposed recently (Xu et al., 2012a, 2012b), has been found to demonstrate larger displacement capacity and provide better bonding compared to hooked-end, deformed and corrugated fibers (Hao and Hao, 2013; Hao et al., 2016).

The impact response of FRC has been investigated in several studies. Banthia et al. (1994) reported that the polypropylene fibers experience dramatic changes in their properties under high rates of tensile loading. The increased sensitivity of the polypropylene fibers at high strain rate loading conditions was believed to be related to a more viscoelastic character of the polypropylene fibers than steel or carbon fibers. Zhang et al. (2005) and Mohammadi et al. (2009) found better crack resistance properties and enhanced energy absorbing capacity of HFRC composite structures against impact. On the basis of drop weight tests performed on steel-polypropylene HFRC, Komlos et al. (1995) and Song et al. (2005) reported positive role of polypropylene fibers in improving the impact resistance of HFRC. This improvement was mainly attributed to the increase the tensile strain capacity of the concrete in the plastic state due to the addition of polypropylene fibers. This was further confirmed by Maalej et al. (2005) for quasi-static tensile tests and by Zhang et al. (2007) for multiple impacts. Almusallam et al. (2013, 2014) highlighted the importance of geometrical properties of fibers in improving the impact resistance of HFRC slabs containing steel, polypropylene and Kevlar fibers. Bindiganavile et al. (2001, 2002) reported the decrease in toughness of SFRC with an increase in the dynamic strain rate observed in drop weight impact tests. This was attributed to the fact that fiber fractures produce a significantly more brittle response in the SFRC as opposed to the fiber pullout mode that is highly energy absorbing, since fiber fractures were observed to occur more commonly at higher strain rates. Their conclusion was further validated by Lok et al. (2003) at even higher strain rates. They reported that the contribution of steel fibers to the toughness of concrete decreases as the strain rate increases. Hao et al. (2016) reported that the spiral steel fibers contribute more significantly to the SFRC beams in dissipating the impact energy than hooked end steel fibers.

Several investigators have studied the dynamic compression response of fiber reinforced concrete (FRC) using Split Hopkinson Pressure Bar (SHPB). Based on tests conducted on steel fiber reinforced concrete (SFRC), Wang et al. (2008) reported significant influence of steel fibers in the softening region of stress–strain curve as compared to their contributions in the initial elastic modulus. Li and Xu (2003, 2009) observed the role of basalt fibers in causing considerable increase in the energy absorption and the deformation capacity of basalt fiber based geopolymeric concrete. Due to the low percentage of fibers, no notable enhancement in dynamic compressive strength was observed. Chen et al. (2009) performed tests on the polyvinyl alcohol (PVA) fiber reinforced ground granulated blast-furnace slag (GGBFS) concrete. The calculations were carried out using the method given in Lok et al. (2002). It was observed that due to the PVA fiber bridging, the toughness of

the concrete materials was significantly increased under dynamic compression. Based on tests conducted on SFRC, Rong et al. (2010) reported significant improvement in its toughness with increase in the fiber percentage as well as the strain rate however no appreciable change was observed in DIF (strength). Wang et al. (2011) reported the bridging effect of fibers in the failure of SFRC. The failure mode of fibrous specimens with highest fiber percentage was essentially a spalling type failure of concrete. Moreover, the toughness energy was proportional to the fiber content under dynamic compression. Liu et al. (2012) investigated experimentally and numerically the comparative influence of steel fibers and rubber fibers/particles in fiber reinforced concrete (FRC) composite on the dynamic compression. Incorporating rubber fibers/particles in the concrete mix in lieu of the fine aggregate resulted in a decrease in the dynamic compressive strength. However, the toughness of the rubber reinforced concrete increased for rubber content up to 10% and a further increase in rubber content caused a decrease in toughness. Zhigang et al. (2012) and Wang et al. (2012) conducted experiments on polyethylene and steel FRC composites. The HFRC composites performed better and had significant strain rate effect as compared to the SFRC. Wang et al. (2010) numerically investigated the dynamic compression behavior of SFRC using finite element analysis. It was reported that the specimen failure was due the combined effect of pressure-dependent plastic hardening and damage softening.

Investigations on the modeling of rate dependent stress-strain behavior of HFRC and engineered cementitious composites are quite limited as compared to modeling of rate dependent behavior of plain concrete (Yang et al., 2015; Lu, 2014; Mohammed et al., 2015; Elsanadedy et al., 2011; Al-Salloum et al., 2014, 2015). Wang et al. (2008) studied the rate dependent stress–strain behavior of SFRC and proposed a model for stress-strain curve based on Weibull function (Weibull, 1951). A simple constitutive model for the DIF (strength) was obtained for GGBFS based concrete by Chen et al. (2013). The models were based on experiments conducted on GGBFS concrete for strain rate range of 10^{-5} to 188 s^{-1}. Su et al. (2014) gave expressions of the DIF (strength) and DIF (critical strain) for ceramic fiber reinforced concrete. However, different equations for different percentage of ceramic fibers were given. Su and Xu (2013) investigated the stress-strain behavior of ceramic fibers reinforced concrete using ϕ 100 mm SHPB apparatus for strain rates of 20 to 130 s^{-1} range. A statistical damage model was proposed and the stress-strain curves were obtained for strain rate range of 28 to 62 s^{-1}. Two different equations for calculating the DIF (strength) were given. DIF (strength) and DIF (toughness) models were given by Hao and Hao (2013) for SFRC containing spiral fibers. However, different models were given for different percentage of steel fibers for both DIF (strength) and DIF (toughness). DIF (strength) models were given by Wu et al. (2010) for copper slag RC under dynamic compression.

It can be seen from the literature that only limited information is available on the dynamic properties of HFRC involving two or more fibers of different material/geometric characteristics. The fiber combinations used in the casting of HFRC composites play an important role in the dynamic response of HFRC composites. In the present study, the HFRC composite specimens were cast by using three types of fibers – hooked steel fibers (SF), monofilament crimped polypropylene fibers (PF) and staple Kevlar fibers (KF). The steel fibers have high elastic modulus, stiffness and toughness properties. Hooked steel fibers generally contribute more to the toughness than straight fibers, because the anchorage with the surrounding matrix is improved by the hooked ends (Taerwe and

Vangysel, 1996; Banthia and Trottier, 1991). Longer fibers and higher aspect ratio also contribute to the higher toughness since the larger contact surface with the matrix results in stronger friction (Banthia and Sappakittipakorn, 2007). The monofilament crimped polypropylene fibers have good ductility, dispersion and help in condensing the microstructure of concrete (Sun and Xu, 2009). The staple Kevlar fibers have better strength, stiffness properties as compared to the steel and polypropylene fibers (Uchida et al., 2010; Nakagawa et al.1989; Burgoyne, 1992).

The present study focuses on the rate dependent behavior of HFRC composites, studied recently for its characterization of static response (Abadel et al., 2015). Experiments were conducted on three fiber combinations based HFRC composites containing single, two and three fiber types with varying volume fractions for strain rates ranging from 25 to 125 s^{-1} using SHPB apparatus. Steel fibers were used in all HFRC composite mixes. A rate dependent model proposed for the stress-strain curve of plain concrete in the earlier study by the authors (Al-Salloum et al., 2015) is extended to incorporate the effect of fibers. The influence of strain rate and the fibers on the rate dependent characteristics of HFRC composites are discussed.

2 EXPERIMENTAL SETUP

The schematic as well as the experimental setup of SHPB is given in Figure 1. The details of the experimental setup are given in authors' earlier paper (Al-Salloum et al., 2015).

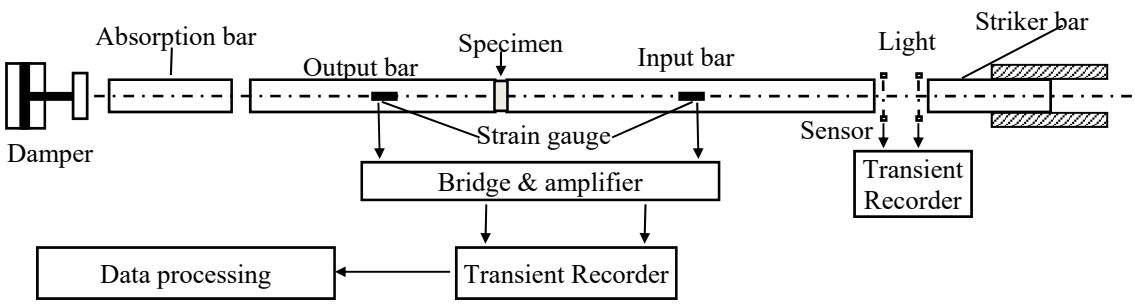

(a)

(b)

Figure 1: SHPB setup: (a) Schematic view; (b) Photograph.

For dynamic compression loading, the specimen can be simply sandwiched between input and output bars. The impact produced through the striker yields a rectangular/trapezoidal compressive stress pulse in the input bar, ε_i. Depending on the physical properties of the sample, part of the stress pulse is reflected back into the input bar as ε_r, and remaining part is transmitted into the output bar as ε_o. The stress pulses are recorded through strain gauges which are located at discrete points on the input and output bars. These pulses are used to generate dynamic compression stress–strain curves. The time histories of strain $\varepsilon(t)$, strain-rate $\dot{\varepsilon}(t)$, and stress $\sigma(t)$, in the specimen at any time t can be obtained from the following equations:

$$\varepsilon(t) = \frac{2C_b}{L} \int_{\omega=0}^{t} \varepsilon_r(\omega) d\omega, \tag{1}$$

$$\dot{\varepsilon}(t) = \frac{2C_b}{L} \varepsilon_r(t), \text{ and} \tag{2}$$

$$\sigma(t) = \frac{A_b E_b}{A_s} \varepsilon_o(t). \tag{3}$$

where E_b is the Modulus of elasticity of Hopkinson bars; A_s and A_b are the cross sectional areas of specimen and Hopkinson bars respectively; C_b is the velocity of longitudinal waves in Hopkinson bars; L is the length of specimen. Using the average of the forces acting on both interface planes:

$$\dot{\varepsilon}(t) = \frac{C_b}{L} \{\varepsilon_o(t) + \varepsilon_i(t) + \varepsilon_r(t)\}, \text{ and} \tag{4}$$

$$\sigma(t) = \frac{A_b E_b}{2A_s} \{\varepsilon_i(t) + \varepsilon_r(t) + \varepsilon_o(t)\}. \tag{5}$$

In the experiments conducted on the HFRC composite specimens, the length of the input bar was 6.0 m whereas the length of the output bar was 4.0 m. The diameter of the input and output bars was 75 mm. The properties of steel bars used in the SHPB set up are: Velocity of longitudinal waves in Hopkinson bars, C_b = 5200 m/s; Young Modulus, E_b = 208 GPa; Density, ρ = 7900 kg/m^3; and Poisson's ratio ν= 0.3. Equations (1), (4) and (5) were used for generating the rate dependent stress-strain plots. The validity of the basic assumptions involved in the above analysis have been investigated earlier (e.g. Verleysen et al., 2009; Marais et al., 2004).

3 EXPERIMENTAL PROGRAM

3.1 Materials

3.1.1 Plain Concrete

Plain concrete (without fibers) was obtained from a local ready-mix plant. Type 1 ordinary Portland cement was used in the preparation of concrete. A mixture of two fine sands was used as fine

aggregates, and crushed limestone with a maximum size of 10 mm was employed as coarse aggregate. Table 1 shows the details of plain concrete mix.

Material	Weight (kg/m^3)
Cement	520
Fine sand	586
Coarse aggregate (Nominal size = 10 mm)	850
Coarse aggregate (Nominal size = 5 mm)	315
Water (water-cement ratio = 0.28)	145
GLI-110 (Super-plasticizer)	3 Liters
Retarder LD10	1.5 Liters

Table 1: Details of plain concrete mix M0 used in the casting of HFRC composite specimens.

3.1.2 Fibers

Steel, Polypropylene and Kevlar fibers were used in the preparation of the HFRC. The steel fibers were hooked ended, the polypropylene fibers were crimped whereas the Kevlar fibers were plain. The material and geometrical properties of the fibers, shown in Figure 2, are given in Table 2. Steel and polypropylene fibers were purchased from the local market, whereas Kevlar fibers were prepared using needle felts of Kevlar. The needled fibers were epoxy wiped for merging the needle felts and then cut to small sizes of 45 mm length.

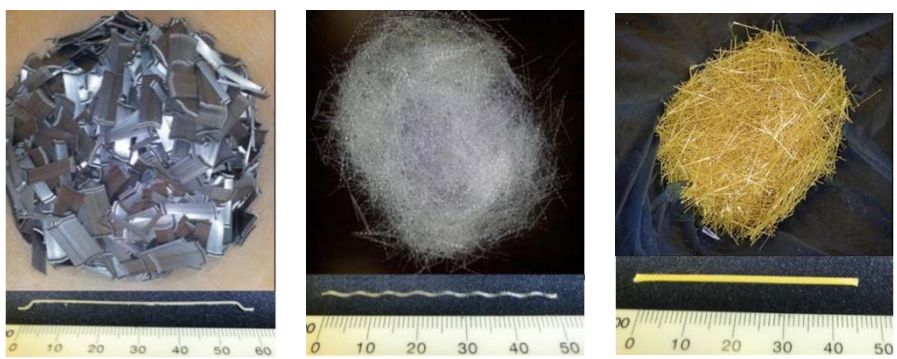

(a) (b) (c)

Figure 2: Fibers used in the study: (a) Hooked-steel fibers; (b) Monofilament crimped polypropylene fibers; (c) Kevlar fibers.

Fibers*	Fiber length (mm)	Fiber diameter/size (mm)	Tensile strength (MPa)	Elastic modulus (GPa)	Specific gravity	Shape
SF	60	0.75 ϕ	1225	200	7.85	Hooked ends
PF	50	1.0 × 0.6 (Rectangular)	550	4	0.9	Crimped
KF	45	0.5 ϕ	3220	131	1.45	Plain

* SF: Steel fibers; PF: Polypropylene fibers; KF: Kevlar fibers

Table 2: Fiber properties and parameters.

3.1.3 HFRC

Besides a control concrete mix (M0), eight mixes of HFRC composite containing different proportions of three types of fibers (mixes M1 to M8) were used in this study. Three fiber combinations consisting of single fibers, two fiber types and three fiber types were considered. Steel fibers were used in all HFRC composite mixes. For two fibers based hybrid, steel with polypropylene and steel with Kevlar were considered whereas for three fibers based hybrid, all three types of fibers were considered. Two total fiber volume fractions of 1.2% and 1.4% were considered in the study. The volume fractions of polypropylene and Kevlar fibers were fixed and were taken as 0.2% and 0.3% respectively whereas the volume fraction of steel fibers was varied from 0.7% to 1.4%. The volume proportions of steel and synthetic fibers used in the HFRC composite mixes are given in Table 3. For the production of HFRC composite, the desired quantity of plain concrete was taken into a small size concrete mixer. The desired quantities of fibers were then added in the mixer, to obtain HFRC composite mixes M1 through M8. The even distribution of fibers was ensured by manual sprinkling of all fibers simultaneously in small dosages during mixing. The total duration of mixing including 2 minutes for adding fibers in concrete was 5 minutes.

3.1.4 Specimens

The specimens were cast using the details of concrete and fibers percentages given in Table 1 and Table 3, respectively. Five cylindrical specimens (Total = 45) with ϕ 73 mm diameter and an aspect ratio of 0.5 (length of specimen = 36.5 mm) of each HFRC composite mix were cast. Three specimens were tested under three different strain rates and the remaining test specimens were used for repeating the tests in which inconsistency was noticed. For each mix, three standard cylindrical specimens (150 × 300 mm) were used for determining quasi-static compressive strength of HFRC mixes.

Concrete Mix ID	Fiber* (percent by volume)			
	PF	SF	KF	Total
M0	0.0	0.0	0.0	0.0
M1	0.0	1.2	0.0	1.2
M2	0.2	1.0	0.0	1.2
M3	0.0	1.4	0.0	1.4
M4	0.2	1.2	0.0	1.4
M5	0.0	0.9	0.3	1.2
M6	0.0	1.1	0.3	1.4
M7	0.2	0.9	0.3	1.4
M8	0.2	0.7	0.3	1.2

* SF: Steel fibers; PF: Polypropylene fibers; KF: Kevlar fibers

Table 3: Fiber volume fractions in different concrete mixes.

4 RESULTS AND DISCUSSION

The HFRC composite specimens were tested under dynamic compression using SHPB apparatus. Variation in strain rate was achieved by using striker bars of varying lengths and by varying the gas pressure. Because of the brittle nature of specimens, relatively long strikers are chosen for the experiments. For relatively lower strain rates, the specimens were tested using 2.2 m long striker at a maintained pressure of 4 bar in the gas gun, whereas for getting the strain rates on the higher side, 1.0 m long striker under a maintained pressure of 6 bar in the gas gun was used. Mid-range strain rates were obtained using 1.0 m striker at 4 bar pressure. The variation of strain rates obtained using the three different striker bars is shown in Table 4. Based on the strain rate values given in Table 4, the testing schemes can be categorized in strain rate ranges: (i) Range 1: 25 – 50 s^{-1} (ii) Range 2: 50 – 100 s^{-1} and (iii) Range 3: 100 – 125 s^{-1}. In the present study, the representative strain rate is the strain rate corresponding to the ultimate stress.

4.1 Failure Mode

Figure 3 shows the damage pattern in selected test specimens, retrived after SHPB testing, for different strain rate ranges. In general, it can be seen from the figure that the degree of damage has increased with the increase of strain rate, irrespective of the presence of different fibers. Relatively large size fragments of the specimens were observed for lower strain rates (Strain rate range 1, Table 4) whereas smaller size and crushed fragments were observed for all the HFRC composite specimens tested at higher strain rates (Strain rate range 3, Table 4). Moreover, for the lower strain rates, vertically cracked specimens were observed, which is quite similar to the failure mode usually associated with static testing. In comparison to the control mix, M0, the specimens containing fibers (M1 to M8) sustain comparatively lower degree of damage.

Concrete Mix ID	Strain rate, $\dot{\varepsilon}$ (s^{-1})		
	2.2 m long striker at 4 bar pressure (Strain rate range 1: 25 – 50 s^{-1})	1.0 m long striker at 4 bar pressure (Strain rate range 2: 50 – 100 s^{-1})	1.0 m long striker at 6 bar pressure (Strain rate range 3: 100 – 125 s^{-1})
M0	36	78	111
M1	32	75	110
M2	26	82	113
M3	25	71	112
M4	30	67	122
M5	26	70	-
M6	31	74	123
M7	31	69	112
M8	33	70	108

Table 4: Observed strain rate values using different striker bars and gas pressure combinations.

This seems to be due to the binding effect and hybrid effect of the different fibers used in the experimental scheme. For the case of HFRC composites made of polypropylene and steel fibers (M2

and M4 mixes), the fragments of the damaged specimens were considerably larger than the fragmented specimens of M1 and M3 mixes. This can be attributed to the synergistic effect of the stiff and flexible fibers in the HFRC composite. Possibly due to the presence of relatively large percentage of stiffer fibers in M7 and M8 mixes, fiber pull out and smaller size fragments were observed for higher strain rates. For the case of moderate strain rate (Strain rate range 2, Table 4), fractured fragments of the concrete matrix bound with fibers were also observed. This is probably due to fiber bridging.

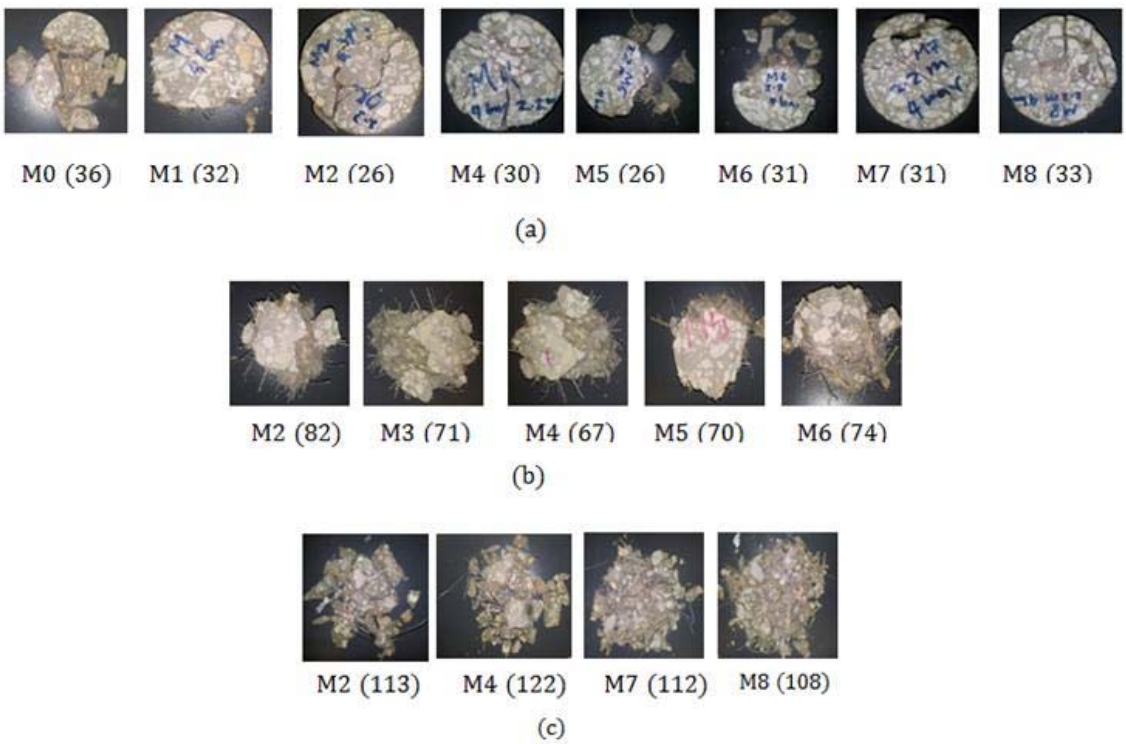

Figure 3: Failure modes of different HFRC specimens retrieved after SHPB testing (Value within brackets is the strain rate in s^{-1}): (a) Strain rate range 1; (b) Strain rate range 2; (c) Strain rate range 3.

4.2 Effect of Fibers on Compressive Strength, Critical Strain and Toughness

In order to study the effect of different fibers on the influence of properties of HFRC composite mixes (M1 to M8) tested under different strain rate ranges (Strain rate range 1: 25 – 50 s^{-1}; Strain rate range 2: 50 – 100 s^{-1}; Strain rate range 3: 100 – 125 s^{-1}), the mixes were divided into the following four groups (Abadel et al., 2015; Almusallam et al. 2015):

Group-1 (M1 and M2): $\left.\begin{matrix}\text{M1:SF alone}\\ \text{M2:SF+PF}\end{matrix}\right\}$ with total fiber volume fraction = 1.2%

Group-2 (M3 and M4): $\left.\begin{matrix}\text{M3:SF alone}\\ \text{M4:SF+PF}\end{matrix}\right\}$ with total fiber volume fraction = 1.4%

Group-3 (M5 and M6): $\left.\begin{matrix}\text{M5:SF+KF with total volume fraction} = 1.2\%\\ \text{M6:SF+KF with total volume fraction} = 1.4\%\end{matrix}\right\}$ KF=0.3%

Group-4 (M7 and M8): $\left.\begin{matrix}\text{M7:SF+PF+KF with total volume fraction} = 1.4\%\\ \text{M8:SF+PF+KF with total volume fraction} = 1.2\%\end{matrix}\right\}$ PF=0.2%,KF=0.3%

The area under the stress-strain curve was calculated to assess the energy absorption capacity or the toughness. The area under the full curve or the area under the curve up to a maximum microstrain value of 30000, whichever is earlier, was considered for calculating the toughness. For the better performing HFRC composite, higher value of toughness is desirable. The critical strain is the strain corresponding to the peak stress. The critical strain is an important parameter in determining the failure. For structures subjected to strain rate loadings, higher value of critical strain is desirable. The DIF for strength, critical strain and toughness were also calculated. Moreover, percent increase/decrease in the values of the dynamic compressive strength, f_{cd}, critical strain, ε_{cd} and the dynamic toughness with respect to the control mix, M0 were also calculated. The failure modes of the HFRC composite specimens (mixes M1 to M8) tested at different strain rates are shown in Figure 3. The salient features of the stress-strain plots are presented in Figure 4 and summarized in Table 5.

For control concrete, M0, the DIF (strength) is increased by almost 14% when the strain rate range changes from 1 to 2. The change of strain range 2 to 3 causes increase of about 17% in the DIF (strength) whereas this increase is 33% when the strain rate range changes from 1 to 3.

The enhancement in the dynamic strength of the fibrous concrete composites (Group 1 to Group 4) is also calculated over the control concrete, M0, tested for the corresponding strain rate range. The percent increase in the dynamic strength is given within brackets in the tenth column of Table 5. The main observations are:

- The addition of lower percentage of steel fibers (M1: 1.2%) results in the increase in the dynamic strength which varies from 12% to 21% at tested strain rate ranges. However, the addition of relatively higher percentage of steel fibers (1.4%, M3) results in an increase of almost 18% to 28% at different strain rate ranges.
- With the addition of 0.2% PF along with 1% steel fibers (M2), the enhancement in dynamic strength ranges from 5% to 12% for different strain rate ranges. The enhancement in dynamic strength ranges from 12% to 18% when 0.2% PF were added along with 1.2% of steel fibers (M4).
- With the addition of 0.3% KF along with 0.9% steel fibers (M5), enhancement in dynamic strength up to 5% for different strain rate ranges is observed whereas, the enhancement in dynamic strength ranges from 2% to 10% when 0.3% KF were added along with 1.1% of steel fibers (M6). The lower value of dynamic strength enhancements in (SF+KF) mixes as compared to the (SF+PF) mixes is mainly due to the variation in the surface profiles of the two fibers.

- The trend of dynamic critical strain and dynamic toughness is qualitatively similar to dynamic strength. However, the quantitative percentage change in the properties is different with some exceptions. The percent enhancements in the dynamic toughness and dynamic critical strain, with respect to the control concrete M0 tested for the corresponding strain rate range, are given within brackets in the 11^{th} and 9^{th} columns of Table 5, respectively.

It can be seen from Figure 4 and Table 5 that with the addition of fibers, the energy absorption capacity or the toughness property of HFRC composites is significantly increased. The maximum toughness enhancement is observed for Group 2 HFRC composites. The scatter in the toughness enhancement for Group 1 and Group 3 mixes is comparable. The average value of toughness enhancement for both Group 1 and Group 3 mixes is found to be around 158%. The average increase in the toughness value of Group 4 mixes is almost 217%. The least performing, as far as the dynamic toughness enhancements are concerned, are the Group 4 mixes. The minimum and the maximum values of the toughness enhancement are 34% (M8, Strain rate range 2) and 191% (M7, Strain rate range 1), respectively. The average toughness enhancement is about 129% for Group 4 mixes. The better performance of mix M4 HFRC composite can be attributed to the hybridizing effect of stiffer (steel) and softer/weaker (polypropylene) fibers. The influence of fibers on the DIF (toughness) is also investigated. It is seen from Figure 4 and Table 5 that different values of DIF (toughness) were obtained for different HFRC composite mixes tested at the same strain rate range. For strain range 3, the DIF (toughness) of M4 HFRC composite tested was almost 7 whereas the DIF (toughness) of M0 mix was almost 5. For the same tested strain rate ranges, the response of M2 HFRC composite and the M4 HFRC composite is comparable. For Group 4 mixes, with the exception of the specimens tested for strain rate range 2, the DIF (toughness) for M7 and M8 mixes are comparable.

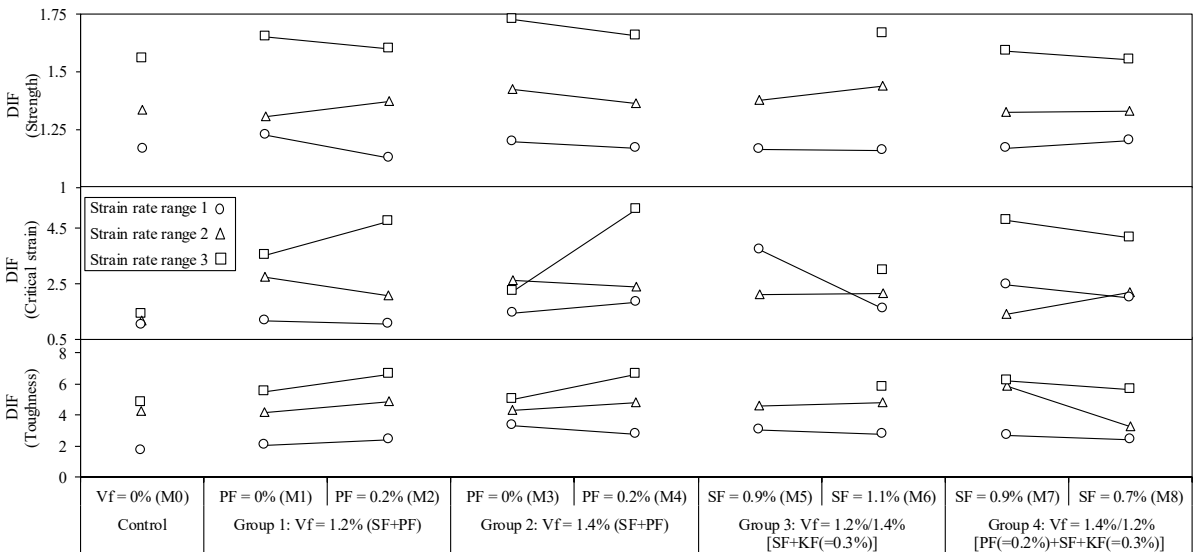

Figure 4: Effect of different fibers on different properties of HFRC mixes tested under three different strain rate ranges. (Vf = Fiber volume; PF = Polypropylene fibers; SF = Steel fibers; KF = Kevlar fibers; Strain rate range 1: 25 – 50 s^{-1}; Strain rate range 2: 50 – 100 s^{-1}; Strain rate range 3: 100 – 125 s^{-1}).

Group	Mix	Reinf. Index, RI_v	Static critical micro-strain, ε_{cs}	Static strength, f_{cs} (MPa)	Static Tough. ($\times 10^6$ MPa)	Strain rate, $\dot{\varepsilon}$ (s^{-1})	Strain rate range	Dyn. Critical micro-strain*, ε_{cd}	Dyn. Strength*, f_{cd} (MPa)	Dyn. Tough.* ($\times 10^6$ MPa)	DIF (Critical Strain)	DIF (Strength)	DIF (Tough.)
(1)	(2)	(3)	(4)	(5)	(6)	(7)	(8)	(9)	(10)	(11)	(12)	(13)	(14)
Control	M0	0.00	2930	64.5	0.46	111	3	4086	100.5	2.18	1.39	1.56	4.77
						78	2	3496	86.0	1.94	1.19	1.33	4.26
						36	1	2980	75.3	0.76	1.02	1.17	1.68
Group 1	M1	0.96	3373	73.5	1.09	110	3	11951 (192%)	121.5(21%)	5.99(175%)	3.54	1.65	5.49
						75	2	9215(164%)	96.0(12%)	4.56(135%)	2.73	1.31	4.19
						32	1	3968(33%)	90.0(19%)	2.27(197%)	1.18	1.22	2.09
	M2	0.80	3233	70.0	0.85	113	3	15424 (277%)	112.1(11%)	5.65(160%)	4.77	1.60	6.62
						82	2	6692(91%)	96.0(12%)	4.16(114%)	2.07	1.37	4.87
						26	1	3419(77%)	79.0(5%)	2.03(166%)	1.06	1.13	2.38
Group 2	M3	1.12	4250	74.4	1.17	112	3	9445(131%)	128.4(28%)	5.92(172%)	2.22	1.73	5.03
						71	2	11244(222%)	106.0(23%)	5.05(160%)	2.65	1.42	4.30
						24	1	6218(223%)	89.0(18%)	3.89(408%)	1.46	1.20	3.31
	M4	0.96	3273	71.9	0.94	122	3	16973 (315%)	119.0(18%)	6.26(188%)	5.19	1.66	6.64
						67	2	7869(125%)	98.0(14%)	4.52(133%)	2.40	1.36	4.79
						30	1	6007(212%)	84.2(12%)	2.59(239%)	1.84	1.17	2.75
Group 3	M5	0.86	2607	65.4	0.86	-	-	-	-	-	-	-	-
						70	2	5556(59%)	90.0(5%)	3.95(104%)	2.13	1.38	4.59
						26	1	9761(406%)	76.2(1%)	2.64(246%)	3.74	1.17	3.07
	M6	1.02	2403	66.0	0.84	123	3	7213(77%)	110.0(9%)	4.83(122%)	3.00	1.67	5.77
						74	2	5231(50%)	95.0(10%)	4.00(106%)	2.18	1.44	4.78
						31	1	3816(98%)	76.5(2%)	2.31(202%)	1.59	1.16	2.76
Group 4	M7	0.86	2919	66.7	0.82	112	3	13952(241%)	106.0(5%)	5.08(133%)	4.78	1.59	6.18
						69	2	4142(18%)	84.4(3%)	4.81(148%)	1.42	1.33	5.86
						31	1	7236(275%)	78.0(4%)	2.22(191%)	2.48	1.17	2.70
	M8	0.70	2681	65.6	0.81	108	3	11202 (174%)	101.9(1%)	4.58(110%)	4.18	1.55	5.65
						70	2	5918(69%)	87.2(1%)	2.64(36%)	2.21	1.33	3.26
						33	1	5390(37%)	79.0(5%)	1.96(156%)	2.01	1.20	2.42

* Value within brackets is the percentage increase with respect to the control, M0 at the corresponding strain rate range (Strain rate range 1: 25 – 50 s^{-1}; Strain rate range 2: 50 – 100 s^{-1}; Strain rate range 3: 100 – 125 s^{-1})

Table 5: Summary of test results of different concrete mixes.

The critical strain is also affected due to the addition of fibers. It can be observed from Figure 4 and Table 5 that there is a large variation in critical strain values for different fibrous concrete mixes in different groups. This tendency is consistent with the typical stress-strain curves of HFRC mixes under dynamic impact loading wherein large plateau regions are observed which extend even up to large strains (~15000 microstrains). The maximum critical strain enhancement is observed for

M4 mix tested for strain rate range 3 (~315%). The average critical strain enhancement for different mixes of Group 2 and Group 3 is comparable. The average critical strain enhancement for M3 and M4 mixes tested at different strain rate ranges is about 200% whereas for M1 and M2 mixes, the increase is almost 150%.

5 ANALYTICAL MODELING

5.1 Equations for Dynamic Compressive Strength, Critical Strain and Toughness

For determining the dynamic compressive strength, f_{cd}, a unified equation for predicting the DIF (strength) has been developed based on the experimental tests conducted on HFRC specimens. The strain rate and the percentage of different fibers are used for obtaining equation of DIF (strength).

Through regression analysis of the experimental data, simple power law expression describing the DIF (strength) of HFRC can be described by the following equation:

$$(\text{DIF})_{strength} = 0.0475 Exp(0.09p_{SF} + 0.11p_{PF} + 0.04p_{KF}) \left(\frac{\dot{\varepsilon}}{\dot{\varepsilon}_s}\right)^{0.22} \quad (6)$$

where p_{SF}, p_{PF} and p_{KF} are the fiber percentages of steel, polypropylene and Kevlar fibers respectively and $\dot{\varepsilon}_s$ is the quasi-static strain rate (= 30 × 10^{-6} s^{-1}). From Eq. (6), f_{cd} can be determined by $f_{cd} = (\text{DIF})_{\text{strength}} f_{cs}$, where f_{cs} is the static compressive strength of concrete.

The DIF (strength) of different HFRC composites obtained using Eq. (6) are compared with the experimentally observed DIF (strength) and the error analysis plot is shown in Figure 5. The average error values are around 6% with a maximum error of approximately 13%. The upper and lower bounds of error are within ±15% range with majority of the data (89%) lying within ±10 % range. The coefficients for different types of fibers obtained in Eq. (6) differ significantly due to the difference in their geometric, surface and mechanical characteristics. It can be seen that the fibers having low tensile strength have higher values of coefficient. Also, the smaller diameter (or equivalent diameter) fibers have higher values of coefficient. It can be seen from Eq. (6) that the coefficient of plain fibers (Kevlar) is significantly smaller than deformed (hooked steel and crimped polypropylene) fibers. This is probably due to the change in the shape of the fibers. However, the effect of other properties like the length of fibers, elastic modulus of fibers on the coefficient is not very apparent. Therefore, a more rational approach is to seek a model which includes the variations in the geometry and mechanical properties in a unified manner.

For HFRC, DIF may also be estimated using the reinforcing index, RI_v, which has been proved to be a suitable parameter in describing the quasi-static mechanical properties of FRC (Nataraja et al.1999; Ezeldin and Balaguru, 1992). Nataraja et al. (1999) have generated the complete stress-strain curve experimentally and proposed an analytical expression similar to Ezeldin and Balaguru (1992), for FRC produced using crimped steel fibers for compressive strength ranging from 30 to 50 MPa. However, due to the use of the steel fibers alone in these studies (Nataraja et al.1999; Ezeldin and Balaguru, 1992), RI_v, needs to be modified for incorporating the effects of material type, shape and mixing of different fibers, as:

$$RI_v = \sum_i^n RI_{vi} \tag{7}$$

where, suffix i is used for fiber type and RI_v is the comprehensive reinforcing index. The value of i taken in this study is 1 for Steel fibers; 2 for Polypropylene fibers and 3 for Kevlar fibers. RI_{vi} is the value of comprehensive reinforcing index, RI_v, for the i^{th} material given by:

$$RI_{vi} = v_{fi} \frac{k_i l_i}{d_i} \left(\frac{f_{ti}}{f_{ts}} \right)^{\alpha} \tag{8}$$

where, v_{fi} is the volume fraction of fibers; k_i is the bond factor of fibers; l_i is the length of fibers; d_i is the diameter (or equivalent diameter for non-circular sections) of fibers; f_{ti} and f_{ts} are the tensile strength of the material of i^{th} fibers and steel fibers respectively. The values of bond factors, k_i, for hooked-end steel, crimped polypropylene and plain Kevlar fibers of this study are taken as 1, 1 and 0.8 respectively. The value of tension stiffness parameter, α, is taken as 0.5. Taking RI_v into consideration, the expression for the DIF (strength) of HFRC obtained through regression analysis of the experimental data is:

$$(\text{DIF})_{strength} = Exp\left(9.9\times10^{-8} \left(\frac{\dot{\varepsilon}}{\dot{\varepsilon}_s} \right) \left(1 + 0.27 {RI_v}^{1.38} \right) \right) \tag{9}$$

The DIF (strength) of different HFRC composites obtained using Eq. (9) is compared with the experimentally observed DIF (strength) and the error analysis has been carried out. It can be seen from Figure 5 that the scatter in values obtained using Eq. (9) is almost similar with that obtained using Eq. (6) and the values are well within ±15% range. For the DIF (critical strain) as well as the DIF (toughness), equations obtained are similar to Eq. (9):

$$(\text{DIF})_{critical\ strain} = Exp\left(5.4\times10^{-8} \left(\frac{\dot{\varepsilon}}{\dot{\varepsilon}_s} \right) \left(1 + 4.5 {RI_v}^{0.38} \right) \right) \tag{10}$$

$$(\text{DIF})_{Toughness} = Exp\left(2.6\times10^{-7} \left(\frac{\dot{\varepsilon}}{\dot{\varepsilon}_s} \right) \left(1 + 1.07 {RI_v}^{0.011} \right) \right) \tag{11}$$

The DIF (critical strain) values of different HFRC composites obtained using Eq. (10) are compared with the experimentally observed DIF (critical strain) values and the error analysis has been carried out. Figures 6(a) and 6(b) show the scatter in the prediction of DIF (critical strain) and DIF (toughness) respectively. It can be seen from Figure 6 that the scatter in the values obtained using Eqs. (10) and (11) is more than the scatter for DIF (strength). However, increase in scatter for DIF (critical strain) and DIF (toughness) models indicate a weak correlation because the most significant role of fibers starts beyond the peak stress when the concrete cracks. This observation is consistent with the conclusions drawn in earlier studies (Nataraja et al.1999; Ezeldin and Balaguru, 1992; Ou et al., 2012).

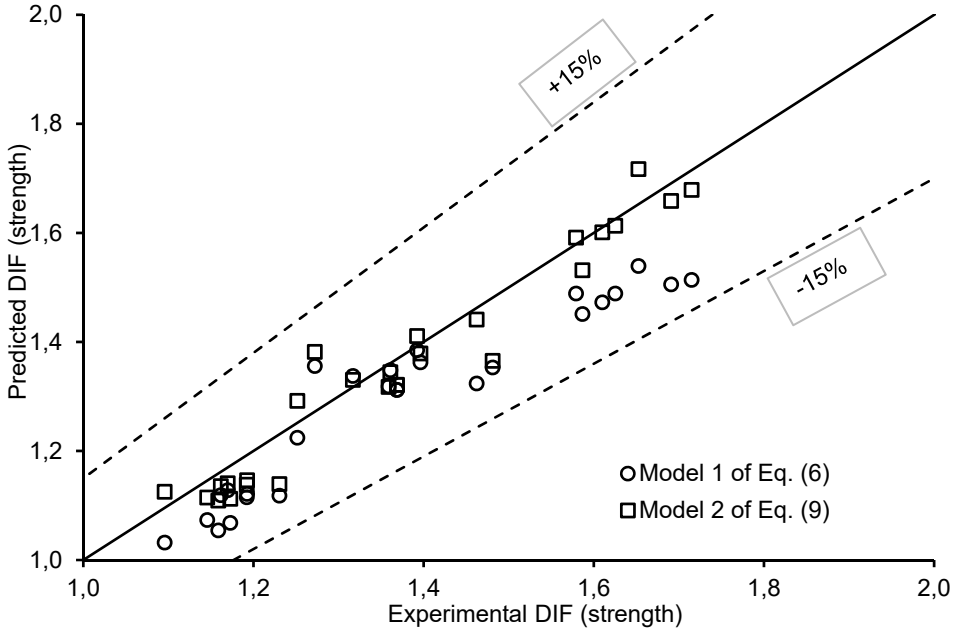

Figure 5: Scatter in the prediction of DIF (strength) using Model 1 of Eq. (6) and Model 2 of Eq. (9).

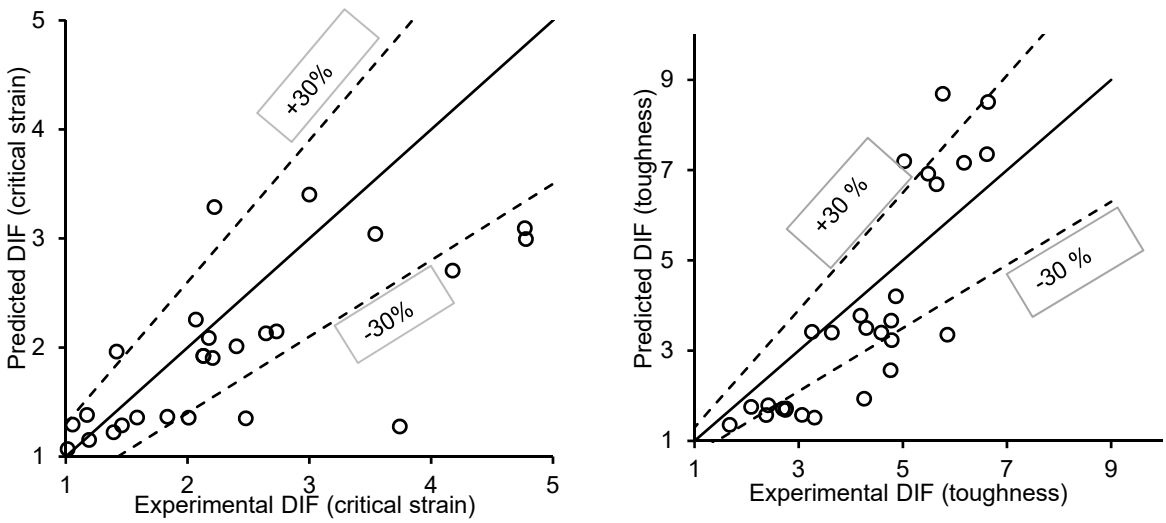

Figure 6: Scatter in the prediction of: (a) DIF (critical strain) using Eq. (10); (b) DIF (toughness) using Eq. (11).

An analytical model for the stress-strain curve, based on the experimental results obtained in the present study is developed. In a previous study carried out by the authors (Al-Salloum et al., 2015), the stress-strain curves for different strain rates of plain concrete were obtained by using a

rational equation comprising of second degree polynomials both in the numerator and the denominator. The equation was given by:

$$Y = \frac{AX + (B-1)X^2}{1 + (A-2)X + BX^2} \tag{12}$$

where A and B parameters are functions of strain rate, $\dot{\varepsilon}$; X and Y are the normalized strain and stress respectively, given by $Y = \sigma / f_{cd}$ and $X = \varepsilon / \varepsilon_{cd}$; where, f_{cd} and ε_{cd} are the peak strength and critical strain components of the stress-strain curve at a given strain rate $\dot{\varepsilon}$; σ is the stress corresponding to the strain ε.

5.2 Derivation of A and B Parameters

In order to ensure no sign change in pre peak zone of stress-strain curve and for ensuring a zero curvature at peak, the constraints for the model used here (i.e. Eq. (12)) are:

$$A(A-2) - B + 1 \geq 0; \text{ and} \tag{13}$$

$$A + B > 1. \tag{14}$$

Moreover, to ensure positive slope of initial tangent, A should be greater than zero. For satisfying these conditions, the parameters A and B are determined in two steps. Firstly, these parameters were obtained individually for different strain rates of each mix by minimizing the error between the experimental and predicted values of stress-strain curves. The values of parameters A and B thus obtained were used to develop models for these parameters in terms of the strain rate and the reinforcing index. The equations obtained for parameters A and B are:

$$A = 3.6Exp\left(9.0\times10^{-8}\left(\frac{\dot{\varepsilon}}{\dot{\varepsilon}_s}\right)\left(1 + 0.01RI_v{}^{0.82}\right)\right) \tag{15}$$

$$B = 0.22Exp\left(3.8\times10^{-7}\left(\frac{\dot{\varepsilon}}{\dot{\varepsilon}_s}\right)\left(1 + 0.002RI_v{}^{0.82}\right)\right) \tag{16}$$

The analytical stress-strain curves of different concrete mixes used in the present study obtained at different strain rates are plotted in Figure 7 along with the smoothed experimental stress-strain curves. The experimental stress-strain curves obtained from the analysis were smoothed using smoothing tools of Matlab. For different groups, the predicted curves match very well with the experimental curves. However, for some mixes, the present model overestimates critical strain values. This can be attributed to the scatter in critical strain model (Eq. 10).

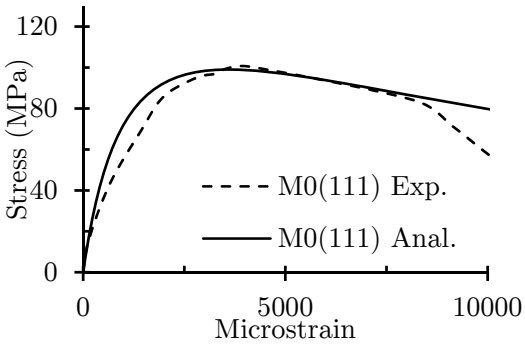
120
80
40
0
Stress (MPa)
M0(111) Exp.
M0(111) Anal.
0
5000
10000
Microstrain

(a)

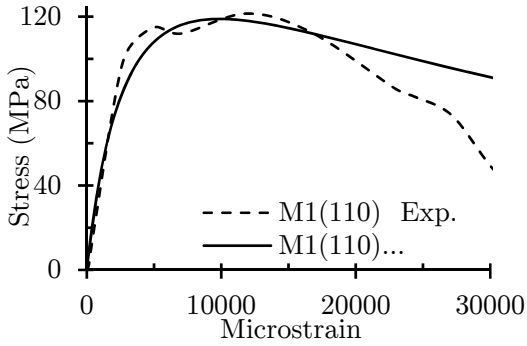
120
80
40
0
Stress (MPa)
M1(110) Exp.
M1(110)...
0
10000
20000
30000
Microstrain

(b)

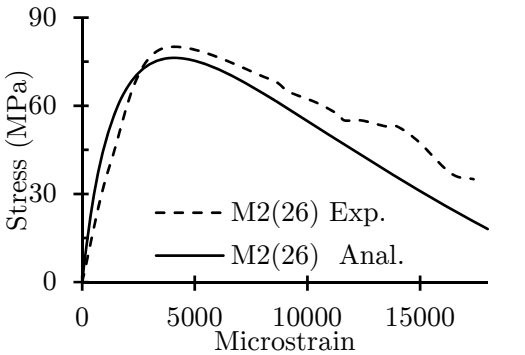
90
60
30
0
Stress (MPa)
M2(26) Exp.
M2(26) Anal.
0
5000
10000
15000
Microstrain

(c)

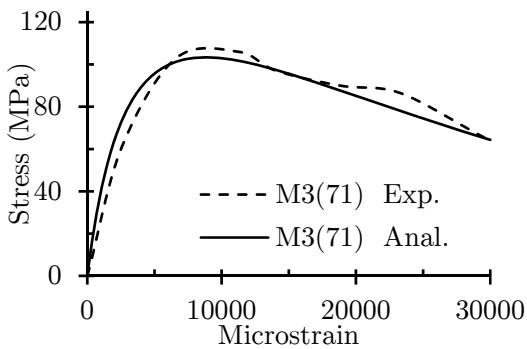
120
80
40
0
Stress (MPa)
M3(71) Exp.
M3(71) Anal.
0
10000
20000
30000
Microstrain

(d)

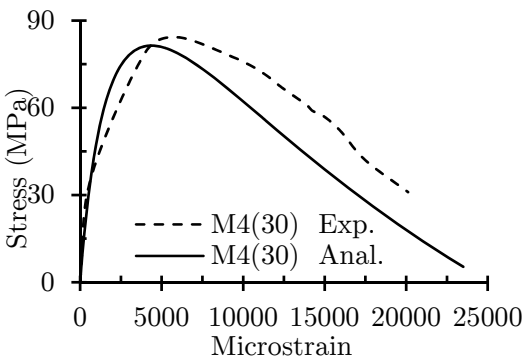
90
60
30
0
Stress (MPa)
M4(30) Exp.
M4(30) Anal.
0
5000
10000
15000
20000
25000
Microstrain

(e)

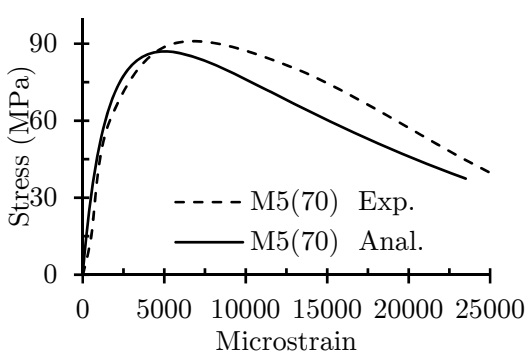
90
60
30
0
Stress (MPa)
M5(70) Exp.
M5(70) Anal.
0
5000
10000
15000
20000
25000
Microstrain

(f)

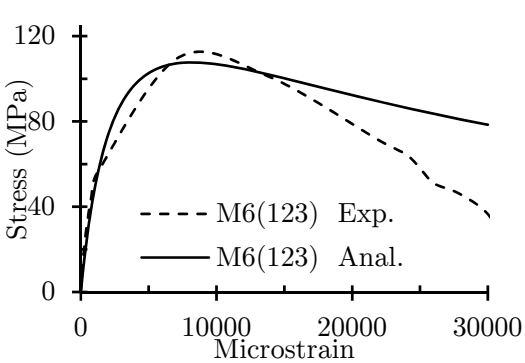
120
80
40
0
Stress (MPa)
M6(123) Exp.
M6(123) Anal.
0
10000
20000
30000
Microstrain

(g)

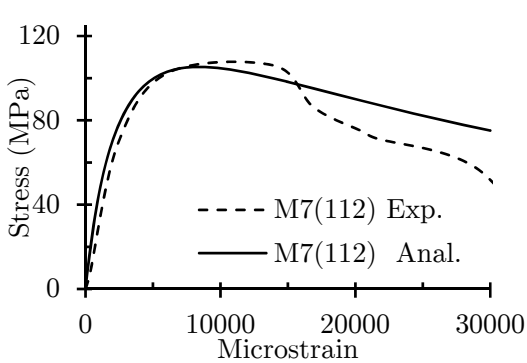
120
80
40
0
Stress (MPa)
M7(112) Exp.
M7(112) Anal.
0
10000
20000
30000
Microstrain

(h)

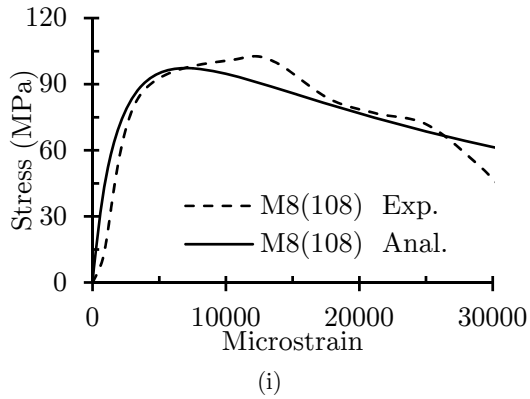

Figure 7: Analytical and experimental stress-strain relationship for different concrete mixes (values given within brackets is strain rate in s^{-1}): (a) Mix M0; (b) Mix M1; (c) Mix M2; (d) Mix M3; (e) Mix M4; (f) Mix M5; (g) Mix M6; (h) Mix M7; (i) Mix M8.

6 CONCLUSIONS

A series of experiments on different HFRC composites made up of different combinations of steel, Kevlar and polypropylene fibers were conducted at varied strain rates using SHPB. The following conclusions are drawn from the study:

- The dynamic behavior of HFRC composites is quite sensitive to the combination of fibers used and helps in improving the mechanical properties of HFRC composites at higher strain rate loadings. The presence of steel fibers in HFRC composites is recommended along with other fibers. Due to the synergistic effect, composites with both stiff and soft fibers perform better than composites having only one type of fibers.
- Taking into account the different parameters tested, it can be seen that the overall performance of mix M4 is superior for dynamic impact loadings. However due to the synergistic effect of composites with both stiff and soft fibers, comparable results are observed for M2 and M7 mixes.
- There is significant improvement in the dynamic toughness of HFRC composites compared to plain concrete specimens.
- Analytical models for DIF (strength), DIF (critical strain) and DIF (toughness) are proposed for HFRC composites. The models are based on the strain rate and a comprehensive reinforcing index for incorporating the effect of fibers. The comprehensive reinforcing index is a function of the material and geometric characteristics of fibers.
- An analytical model is developed for predicting complete stress-strain curves of HFRC composites. The parameters required for the model are based on reinforcing index of hybrid fibers and strain rate. The analytical model gives an adequate estimate of stress–strain curve of HFRC composites under strain rates ranging from 25 to 125 s^{-1}.

Acknowledgements

This work is based on the project funded by the National Plan for Science, Technology and Innovation (MAARIFAH), King Abdulaziz City for Science and Technology, Kingdom of Saudi Arabia, Award Number (12-ADV2619-02).

References

Abadel, A., Abbas, H., Almusallam, T., Al-Salloum, Y., Siddiqui, N. (2015). Mechanical properties of hybrid fiber reinforced concrete – Analytical modeling and experimental behavior. Magazine of Concrete Research. http://dx.doi.org/10.1680/jmacr.15.00276.

Abou El-Mal H.S.S., Sherbini, A.S., Sallam, H.E.M. (2015). Mode II Fracture Toughness of Hybrid FRCs. International Journal of Concrete Structures and Materials 1-12. DOI 10.1007/s40069-015-0117-4.

Ahmed, S.F.U., Maalej, M., Paramasivam, P. (2007). Flexural responses of hybrid steel polyethylene fiber reinforced cement composites containing high volume fly ash. Construction and Building Materials 21:1088-1097.

Almusallam, T.H., Abadel, A.A., Al-Salloum, Y.A., Siddiqui, N.A., Abbas, H. (2015). Effectiveness of hybrid-fibers in improving the impact resistance of RC slabs. International Journal of Impact Engineering 81:61-73.

Almusallam, T.H., Siddiqui, N.A., Iqbal, R.A., Abbas, H. (2013). Response of hybrid-fiber reinforced concrete slabs to hard projectile impact. International Journal of Impact Engineering 58:17–30.

Al-Salloum, Y., Almusallam, T., Ibrahim SM., Abbas, H., Alsayed, S. (2015). Rate dependent behavior and modeling of concrete based on SHPB experiments. Cement and Concrete Composites 55:34–44.

Al-Salloum, Y., Alsayed, S., Almusallam, T., Ibrahim, S.M., Abbas, H. (2014). Investigations on the influence of radial confinement in the impact response of concrete. Computers and Concrete 14(6):675-694.

Banthia, N., Chokri, K., Ohama, Y., Mindess, S. (1994). Fiber-reinforced cement based composites under tensile impact. Advanced Cement Based Materials 1(3):131-141.

Banthia, N., Sappakittipakorn, M. (2007). Toughness enhancement in steel fiber reinforced concrete through fiber hybridization. Cement and Concrete Research 37(9):1366-1372.

Banthia, N., Trottier, J.F. (1991).Deformed steel fiber-cementitious matrix bond under impact. Cement and Concrete Research 21(1):158-168.

Bindiganavile, V., Banthia, N. (2001). Polymer and steel fiber-reinforced cementitious composites under impact loading - part 2: Flexural toughness. ACI Materials Journal 98(1):17-24.

Bindiganavile, V., Banthia, N., Aarup, B. (2002). Impact response of ultra-high-strength fiber-reinforced cement composite. ACI Materials Journal 99(6):543-548.

Bolander, J.E., Choi, S., Duddukuri, S.R. (2008). Fracture of fiber-reinforced cement composites: effects of fiber dispersion. International Journal of Fracture 154:73–86.

Burgoyne, CJ. (1992). Aramid fibres for civil engineering applications, in Construction Materials Reference Book, (ed. Doran DK Cather B), Butterworths.

CEB Comité Euro-International du Béton. CEB-FIP model code 1990.

Chen, P.W., Chung, D.D.L. (1996). Comparative study of concretes reinforced with carbon, polyethylene, and steel fibers and their improvement by latex addition. ACI Material Journals 93(2):129-133.

Chen, Z., Yang, Y., Yao, Y. (2013). Quasi-static and dynamic compressive mechanical properties of engineered cementitious composite incorporating ground granulated blast furnace slag. Materials & Design 44:500–508.

Elsanadedy, H.M., Almusallam, T.H., Abbas, H., Al-Salloum, Y.A., Alsayed, S.H. (2011). Effect of blast loading on CFRP-Retrofitted RC columns – a numerical study. Latin American Journal of Solids and Structures 8:55-81.

Ezeldin, A.S., Balaguru, PN. (1992). Normal- and high-strength fiber-reinforced concrete under compression. Journal of Materials in Civil Engineering 4(4):415-429.

Hao, Y., Hao, H. (2013). Dynamic compressive behaviour of spiral steel fibre reinforced concrete in split Hopkinson pressure bar tests. Construction and Building Materials 48:521–532.

Hao, Y., Hao, H., Chen, G. (2016). Experimental investigation of the behaviour of spiral steel fibre reinforced concrete beams subjected to drop-weight impact loads. Materials and Structures 49: 353-370.

Komlos, K., Babal, B., Nürnbergerová, T. (1995). Hybrid fibre-reinforced concrete under repeated loading. Nuclear Engineering and Design 156(1-2):195-200.

Li, V.C. (2012). Tailoring ECC for Special Attributes: A Review. International Journal of Concrete Structures and Materials 6:135–144.

Li, W., Xu, J. (2009). Mechanical properties of basalt fiber reinforced geopolymeric concrete under impact loading. Materials Science and Engineering: A 505:178–186.

Li, W., Xu, J. (2009). Impact characterization of basalt fiber reinforced geopolymeric concrete using a 100-mm-diameter split Hopkinson pressure bar. Materials Science and Engineering: A 513–514:145–153.

Liu, F., Chen, G., Li, L., Guo, Y. (2012). Study of impact performance of rubber reinforced concrete. Construction and Building Materials 36:604–616.

Lok, T.S., Li, X.B., Zhao, P.J. (2002) Testing and response of large diameter brittle materials subjected to high strain rate. Journal of Materials in Civil Engineering 14:262-269.

Lok, T.S., Zhao, P.J., Lu, G. (2003). Using the split hopkinson pressure bar to investigate the dynamic behaviour of SFRC. Magazine of Concrete Research 55(2):183-190.

Lu, Y. (2014). Dynamic compressive behavior of recycled aggregate concrete based on split Hopkinson pressure bar tests. Latin American Journal of Solids and Structures 11:131-141.

Maalej, M., Quek, S.T., Zhang, J. (2005).Behavior of hybrid-fiber engineered cementitious composites subjected to dynamic tensile loading and projectile impact. Journal of Materials in Civil Engineering 17:143-152.

Marais, S.T., Tait, R.B., Cloete, T. J., Nurick, G.N. (2004). Material testing at high strain rate using the split Hopkinson pressure bar. Latin American Journal of Solids and Structures 1(3):319–339.

Markovic, I. (2006). High-performance hybrid-fibre concrete: Development and utilization. PhD Thesis, Delft University of Technology; Delft University Press, Netherlands.

Mohammadi, Y., Azad, C.R., Singh, S.P., Kaushik, S.K. (2009). Impact resistance of steel fibrous concrete containing fibres of mixed aspect ratio. Construction and Building Materials 23:183–189.

Mohammed, H.J., Zain, M.F.B.M. (2015). Concrete road barrier subjected to impact loads: An overview. Latin American Journal of Solids and Structures 12:1824-1858.

Nakagawa, H., Akihama, S., Suenaga, T. (1989). Mechanical properties of various types of fibre reinforced concretes. International Conference on Recent Developments of Fibre Reinforced Cements and Concretes, Cardiff, UK.

Nataraja, M.C., Dhang, N., Gupta, A.P. (1999) Stress-strain curves for steel-fiber reinforced concrete in compression. Cement and Concrete Composites 21(5-6):383-390.

Ou, Y., Tsai, M., Liu, K., Chang, K. (2012). Compressive behaviour of steel-fiber-reinforced concrete with a high reinforcing index. Journal of Materials in Civil Engineering 24(2):207-215.

Rong, Z., Sun, W., Zhang, Y. (2010). Dynamic compression behavior of ultra-high performance cement based composites. International Journal of Impact Engineering 37:515–520.

Song, P.S., Wu, J.C., Hwang, S., Sheu, B.C. (2005). Statistical analysis of impact strength and strength reliability of steel-polypropylene hybrid fiber-reinforced concrete. Construction and Building Materials 19(1):1-9.

Su, H., Xu, J. (2013). Dynamic compressive behavior of ceramic fiber reinforced concrete under impact load. Construction and Building Materials 45:306–313.

Su, H., Xu, J., Ren, W. (2014). Mechanical properties of ceramic fiber-reinforced concrete under quasi-static and dynamic compression. Materials & Design 57:426–434.

Sun, Z., Xu, Q. (2009). Microscopic, physical and mechanical analysis of polypropylene fiber reinforced concrete. Materials Science and Engineering: A 527:198–204.

Taerwe, L., Vangysel, A. (1996) Influence of steel fibers on design stress-strain curve for high-strength concrete. Journal of Engineering Mechanics -ASCE 122:695-704.

Uchida, Y., Takeyama, T., Dei, T. (2010). Ultra high strength fiber reinforced concrete using aramid fiber. Proceedings of FraMCoS-7, Jeju, South Korea 1492 – 1496.

Verleysen, P., Verhegghe, B., Verstraete, T., Degrieck, J. (2009). Numerical study of the influence of the specimen geometry on split hopkinson bar tensile test results. Latin American Journal of Solids and Structures 6(3):285-298.

Wang, S., Zhang, M.H., Quek, S.T. (2012). Mechanical behavior of fiber-reinforced high-strength concrete subjected to high strain-rate compressive loading. Construction and Building Materials 31: 1–11.

Wang, Z.L., Liu, Y.S., Shen, R.F. (2008).Stress–strain relationship of steel fiber-reinforced concrete under dynamic compression. Construction and Building Materials 22:811–819.

Wang, Z.L., Shi, Z.M., Wang, J.G. (2011). On the strength and toughness properties of SFRC under static-dynamic compression. Composites Part B: Engineering 42:1285–1290.

Wang, Z.L., Wu, L.P., Wang, J.G. (2010). A study of constitutive relation and dynamic failure for SFRC in compression. Construction and Building Materials 24:1358–1363.

Weibull, W. (1951). A statistical distribution function of wide applicability. Journal of Applied Mechanics 18:292–7.

Wu, W., Zhang, W., Ma, G. (2010). Mechanical properties of copper slag reinforced concrete under dynamic compression. Construction and Building Materials 24:910–917.

Xu, Z., Hao, H., Li, H.N. (2012a). Dynamic tensile behaviour of fibre reinforced concrete with spiral fibres. Materials and Design 42:72–88.

Xu, Z., Hao, H., Li, H.N. (2012b). Mesoscale modelling of dynamic tensile behaviour of fibre reinforced concrete with spiral fibres. Cement and Concrete Research 42(11):1475–1493.

Yang, F., Ma, H., Jing, L., Zhao, L., Wang, Z. (2015). Dynamic compressive and splitting tensile tests on mortar using split Hopkinson pressure bar technique. Latin American Journal of Solids and Structures 12:730-746.

Yu, R., Tang, P., Spiesz, P., Brouwers, H.J.H. (2014). A study of multiple effects of nano-silica and hybrid fibres on the properties of Ultra-High Performance Fibre Reinforced Concrete (UHPFRC) incorporating waste bottom ash (WBA). Construction and Building Materials 60:98–110.

Zhang, J., Maalej, M., Quek, S.T. (2007). Performance of hybrid-fiber ECC blast/shelter panels subjected to drop weight impact. Journal of Materials in Civil Engineering 19(10):855-863.

Zhang, M.H., Shim, V.P.W., Lu ,G., Chew, C.W. (2005). Resistance of high strength concrete to projectile impact. International Journal of Impact Engineering 31:825-41.

Zhigang, R., Meng, C., Zhean, L., Weiguo, X. (2012). Dynamic mechanical property of hybrid fiber reinforced concrete (HFRC). Journal of Wuhan University of Technology – Mater. Sci. Ed. 27(4):783-788.